Chemical Engineering Journal 165 (2010) 46–55

Contents lists available at ScienceDirect

Chemical Engineering Journal

journal homepage: www.elsevier.com/locate/cej

Effects of chitosan membrane morphology on copper ion adsorption

A. Ghaee [a], M. Shariaty-Niassar [a,*], J. Barzin [b], T. Matsuura [c]

[a] Department of Chemical Engineering, University College of Engineering, Tehran University, P.O. Box 11365-4563, Tehran, Iran
[b] Department of Biomaterials, Iran Polymer and Petrochemical Institute, P.O. Box 14965/115, Tehran, Iran
[c] Industrial Membrane Research Laboratory, Department of Chemical and Biological Engineering, University of Ottawa, Ottawa, Ont., Canada K1N 6N5

ARTICLE INFO

Article history:
Received 14 June 2010
Received in revised form 19 August 2010
Accepted 22 August 2010

Keywords:
Adsorption
Chitosan
Copper
Morphology
Porosity
Roughness

ABSTRACT

The effect of chitosan membrane morphology on copper ion adsorption was investigated in this work. Dense and macroporous chitosan membranes with various polymer concentrations and silica to chitosan ratios were prepared. The membrane surfaces and cross-section morphologies were characterized by SEM and AFM, and the porosity of macroporous membranes was measured relative to dense membranes. Adsorption experiments were performed in batch processes; also sorption isotherms and kinetics were studied. Increasing the polymer concentration during membrane preparation resulted in increased copper adsorption. Increasing the silica to chitosan ratio resulted in greater membrane porosity and surface roughness, which made more amino groups accessible and therefore increased copper sorption. The membrane with the greatest porosity and membrane roughness could adsorb copper in the amount of 5.9 mg/g, the highest amount achieved at an initial copper concentration of 125 ppm. Due to its enhanced roughness, the membrane with a 3/1 silica to chitosan ratio had an active surface area that was nearly doubled compared to dense membrane.

1. Introduction

Heavy metal contamination exists in aqueous waste streams of many industries, such as metal plating, mining operations, electroplating and the pharmaceutical industry. The soil surrounding these sites is also polluted and can contaminate groundwater and surface water. Heavy metals are not biodegradable and tend to accumulate in living organisms, causing various diseases and disorders [1–4]. Copper pollution is of particular concern. While copper plays an essential role in animal metabolism, it is toxic at high concentrations, with effects including vomiting, cramps, convulsions and even death [5].

Treatment processes for metal contaminated waste streams include chemical precipitation, membrane processes, reverse-osmosis, ion exchange, carbon adsorption and co-precipitation/adsorption. Adsorption is one of the few techniques that can remove even trace quantities of metal ions from water. Biosorption is also cost-effective due to a high availability of biosorbent materials in nature and from certain industrial waste streams, and their ability to be easily regenerated.

Chitosan is a biopolymer produced by alkaline *N*-deacetylation of chitin, widely found in the exoskeletons of shellfish and crustaceans. The growing need for new sources of low-cost adsorbent, the increased problems of waste disposal, the increasing cost of synthetic resins and finally high ability of chitosan for metal sorption, undoubtedly make chitosan one of the most attractive materials for wastewater treatment [6]. Chitosan has amine and hydroxyl functional groups that are involved in adsorption. Both nitrogen and oxygen atoms have a lone pair or lone pairs of electrons that can bind a proton or a metal ion through an electron pair sharing to form a complex. Because of the stronger attraction of the lone pair of electrons to the nucleus in an oxygen atom than in a nitrogen atom, the nitrogen atoms would have a greater tendency to donate the lone pair of electrons for sharing with a metal ion to form a metal complex than the oxygen atoms. Amine groups are thus responsible for the uptake of metal cations by a chelation mechanism as follows [7,8]:

$$\text{R-NH}_2 + \text{H}^+ \rightarrow \text{R-NH}_3{}^+ \quad (1)$$

$$\text{R-NH}_2 + \text{Cu}^{2+} \rightarrow \text{R-NH}_2\text{Cu}^{2+} \quad (2)$$

$$\text{R-NH}_3{}^+ + \text{Cu}^{2+} \rightarrow \text{R-NH}_2\text{Cu}^{2+} + \text{H}^+ \quad (3)$$

Chitosan can be used as a sorbent in adsorption columns or in membrane processes. The use of adsorption columns for water decontamination is limited due to high capital and energy costs as well as unfavorable hydrodynamic properties. Therefore, membrane processes have attracted greater attention and are known to be more appropriate for the removal of metal ions.

* Corresponding author. Tel.: +98 2166957785; fax: +98 2166957781.
E-mail addresses: mshariat@ut.ac.ir, azadeh_ghaee@yahoo.com (M. Shariaty-Niassar).

1385-8947/$ – see front matter © 2010 Elsevier B.V. All rights reserved.
doi:10.1016/j.cej.2010.08.051

Nomenclature

A	cross-sectional area of the surface (nm^2)
a	length of the side of the top surface (mm)
b	length of the side of the top surface (mm)
C_0	initial concentration of metal ion in the liquid phase (mg/L)
C_{eq}	equilibrium concentration of metal ion in the liquid phase (mg/L)
k_1	rate constant of pseudo-first order sorption (1/min)
k_2	rate constant of pseudo-second order sorption ($g\,mg^{-1}\,min^{-1}$)
K_F	Freundlich isotherm constant ($mg^{1-1/n}\,g^{-1}\,L^{1/n}$)
K_L	Langmuir isotherm constant (L/g)
m	amount of chitosan membrane (g)
Mi–j	membrane with polymer concentration of i and silica to chitosan ratio of j
n	Freundlich isotherm constant
N	number of experimental data
q	adsorption amount (mg/g)
q_{cal}	calculated sorption amount by applied isotherm (mg/g)
q_e	sorption amount at equilibrium (mg/g)
q_{exp}	experimental adsorption amount (mg/g)
q_m	maximum adsorption capacity (mg/g)
q_t	sorption amount at time t (mg/g)
S_a	average roughness (nm)
S_q	root mean square (rms) roughness (nm)
S_{dq}	root mean square gradient
S_{dr}	developed interfacial area ratio (%)
S_z	average height of the five highest local maximums plus the average height of the five lowest local minimums (nm)
t	time (min)
V	volume of the solution (L)
V_m	membrane volume
z	membrane thickness (mm)
$Z(x,y)$	height function of the area (nm)
ρ_{MP}	macroporous membrane density (g/L)
ρ_D	dense membrane density (g/L)

Most of the studies dedicated to metal ion sorption on chitosan membranes focus on equilibrium models to investigate sorption behaviour [9–11]. In some studies, influences of metal type, metal concentration, temperature and pH on the metal sorption are also considered [9–19].

Most of these studies concentrate on dense membranes for applications other than metal removal, such as drug delivery. These dense membranes have low porosity, which limits diffusion and flux in a continuous process. To increase the porosity of chitosan membranes, porogens such as NaCl or silica gel can be added to the casting solution. After membrane preparation, differences in the solubility of porogens compared to chitosan in some agents like water or sodium hydroxide allow the porogen to be dissolved [16,20–24]. Beppu et al. [16] examined the effect of porosity (calculated by water sorption) in chitosan membranes functionalized with histidine and found out that membranes with higher porosity showed increased capacities of Cu(II) adsorption. Chao et al. [21] investigated the effects of pore size, porosity and crystallinity of chitosan membranes on adsorption of dye and copper ions from waste water. They observed that porosity have strong direct effects on adsorption rate but the effect of membrane morphology was not considered.

In addition to porosity, a membrane's adsorption potential is dependent on its morphology and roughness – these parameters determine the active surface area for adsorption. Knowledge of how these parameters are controlled during membrane formation is necessary in order to make improvements to membrane properties [25]. Zeng and Ruckenstein [24] and Santos et al. [20] investigated surface and cross-section morphology by SEM, but the effect of chitosan membrane morphology on metal adsorption was not studied. The present study investigates the effects of porogen on the porosity, morphology, and roughness of chitosan membranes, and evaluates the impact of these parameters on copper ion adsorption.

2. Material and methods

2.1. Materials

Chitosan having a deacetylation degree of 90% was purchased from Chitotech. All other chemicals (glutaraldehyde, acetic acid, sodium hydroxide, cupric sulfate) were of analytical grade used without further purification. Chromatography silica gels (15–40 μm) were obtained from Merck. The solutions were prepared using distilled water.

2.2. Membrane preparation

Membranes were prepared by dissolving chitosan at final concentrations of 3%, 4.5%, or 6% (w/w) in 10% aqueous acetic acid solution.

For dense membrane preparation, the solution was poured onto a flat polycarbonate surface following aeration. A proper membrane thickness was formed by using a film applicator and the membranes were dried at room temperature for 24 h. The membranes were then immersed in an aqueous solution of sodium hydroxide (1 M) for 24 h, and then washed with distilled water.

For macroporous membranes, chitosan solutions were mixed with silica gel as the porogen at silica/chitosan weight ratios of 1/1 and 3/1. These ratios are selected from Zeng and Ruckenstein's research [24] to have higher flow rate and mechanical stability in continuous processes. Membranes with the same thickness as dense membranes were casted and dried at room temperature for 24 h. Then the membranes were immersed in an aqueous solution of sodium hydroxide (1 M) for 24 h to dissolve silica particles and finally the membranes were washed with distilled water [24].

2.2.1. Membrane crosslinking

Prior to dissolving chitosan in acidic media, it must be crosslinked to prevent polymer degradation. Chitosan can be crosslinked with bifunctional chemicals such as glutaraldehyde and epichlorohydrin, which react (through Schiff's base reaction) [9,17].

Natural chitosan membranes were heterogeneously crosslinked by 0.25% (w/w) aqueous glutaraldehyde solution. This value was selected from Hsien et al.'s research [26]. 3.0 g of wet chitosan membrane was immersed in 50 mL of glutaraldehyde solution (the molar ratio of glutaraldehyde to chitosan is 50) at a temperature of 25 °C for 30 min, followed by washing with distilled water to remove the unreacted glutaraldehyde residues. At the final stage the membranes were dried with filter paper.

2.3. Adsorption experiments

Chitosan has stronger ability to adsorb Cu^{2+} from $CuSO_4$ compared to other salts [7,17]. Therefore, copper solutions were prepared by dissolving hydrated copper sulfate ($CuSO_4{\cdot}5H_2O$) in water to a concentration of 125 ppm. Batch adsorption experiments were carried out by soaking 2 cm × 3 cm (wet base) of crosslinked chitosan membrane in 50 mL of copper solution over 24 h at 20 °C

with magnetic stirring, followed by the measurement of copper concentration in the solution using a flame atomic absorption spectrophotometer. This adsorption period is sufficient to reach adsorption equilibrium as shown later by kinetic experiments.

The amount of adsorbate in solid phase (q (mg/g)) is calculated by the following expression:

$$q = (C_0 - C_{eq}) \times \frac{V}{m} \quad (4)$$

where C_0 and C_{eq} are the initial and equilibrium concentrations of metal ion in the liquid phase (mg/L), respectively, V is the volume of the solution (L) and m is the amount of chitosan membrane (g).

Adsorption isotherms illustrate the adsorbate distribution between the solid and liquid phase and are obtained by varying experimental parameters such as the initial concentration of metal. Adsorption isotherms were obtained using initial metal concentrations of 62.5, 125, 250, 500, 1000 mg/L for dense and macroporous chitosan membrane prepared from the dope with a polymer concentration of 6%.

Adsorption kinetic studies were performed for chitosan membranes (prepared from the dope with polymer concentration of 6%) with an initial copper concentration of 250 ppm.

2.4. Membrane reuse

The use of chitosan for metal recovery can be limited by the cost of the polymer compared to other waste materials, so the recycling of adsorbent is an important step in process design. Dense and macroporous chitosan membranes (2 cm × 3 cm) were immersed to 50 mL of copper solution with initial concentration of 250 ppm at pH 5, 20 °C and 150 rpm stirring rate for 24 h, followed by washing with distilled water to remove any unadsorbed metal. The membranes were then kept in 30 mL of 10^{-4} M EDTA solution under stirring for 24 h, to regenerate the membrane by removing the adsorbed metal. (This set of the first adsorption/desorption procedure is called the first cycle.) Second and third cycles were performed with the membrane used in the foregoing cycle. Procedures in these cycles were the same as first one. The copper concentration in solution was measured by atomic absorption spectrometry.

Metal desorption percentage for each cycle was calculated using the following expression:

$$\text{Desorption\%} = \frac{\text{amount of metal desorbed}}{\text{amount of metal adsorbed}} \times 100 \quad (5)$$

2.5. Characterization

2.5.1. ATR-FTIR

ATR-FTIR analysis (Bruker, EQUINOX 55) was used to characterize the surface chemistry of membranes made of natural, crosslinked and macroporous chitosan membrane before and after adsorption.

2.5.2. Membrane thickness and porosity

Relative membrane porosity was measured by comparing the density of a macroporous membrane to that of a dense membrane prepared from the same chitosan solution. Porosity of the macroporous membrane was calculated by the following equation [27]:

$$\text{Membrane porosity} = \left(1 - \frac{\rho_{MP}}{\rho_D}\right) \times 100 \quad (6)$$

where ρ_{MP} and ρ_D are macroporous and dense membrane densities, respectively. ρ_{MP} was calculated by the relation between the macroporous membrane dry weight (W) and volume (V). The macroporous membrane dry weight was obtained by drying procedures in oven until constant weight. The volume of membrane (V_m) was calculated by following equation:

$$V_m = a \times b \times z \quad (7)$$

where a and b are the length of the sides of the top surface (mm) and z is the membrane thickness (mm) which was measured by SEM. ρ_D was obtained by the same method, replacing the macroporous membrane by the dense membrane. Five samples were used for each dense and porous membrane used in this research.

2.5.3. Scanning electron microscopy – energy dispersive X-ray spectroscopy

For cross-section analysis, membranes were fractured in liquid nitrogen before their surfaces (including the fractured cross-sections) were covered with a thin layer of gold using a sputter coater (SCDOOS – Baltec, Switzerland). The cross-sections were then observed with a scanning electron microscope (SEM) coupled with an energy dispersive X-ray spectroscopy (EDX), (XL30-Philips-Netherlands).

2.5.4. Atomic force microscopy

Top and bottom surface morphology of dense and macroporous membranes (with polymer concentration of 6%) were characterized with AFM (Dualscope/Rasterscope C26, DME, Denmark) in noncontact mode. Various roughness parameters can be measured by AFM. Some of these are reported in this work; the definitions of these parameters are as follows [28,29]:

S_z is the average height of the five highest local maximums plus the average height of the five lowest local minimums.

S_a is the average roughness evaluated over the complete surface and defined as:

$$S_a = \iint_a |Z(x,y)| \cdot dx \cdot dy \quad (8)$$

where Z is the height function of the area.

S_q is the root mean square (rms) roughness expressed as follows:

$$S_q = \sqrt{\iint_a |Z(x,y)|^2 \cdot dx \cdot dy} \quad (9)$$

The average surface roughness and root mean square roughness data indicate significant deviations in texture characteristics.

S_{dq} (root mean square gradient) defines the slope for each point of area excluding points on the edge and is calculated as follows:

$$S_{dq} = \sqrt{\frac{1}{A}\int_0^{lx}\int_0^{ly}\left(\left(\frac{\partial Z(x,y)}{\partial x}\right)^2 + \left(\frac{\partial Z(x,y)}{\partial y}\right)^2\right) \cdot dx \cdot dy} \quad (10)$$

where A is the cross-sectional area.

S_{dr} (developed interfacial area ratio) is the increase in surface area in relation to a flat surface covering the same area in the X/Y plane. A value of 100% means that the area is double that of the flat surface.

$$S_{dr} = \frac{\text{Texture surface area} - \text{Cross-sectional area}}{\text{Cross-sectional area}} \quad (11)$$

2.5.5. Atomic absorption experiments

The concentrations of metal ions were measured using a flame atomic absorption spectrophotometer (Varian AA 240). All reported copper concentrations are the mean value of three replicates.

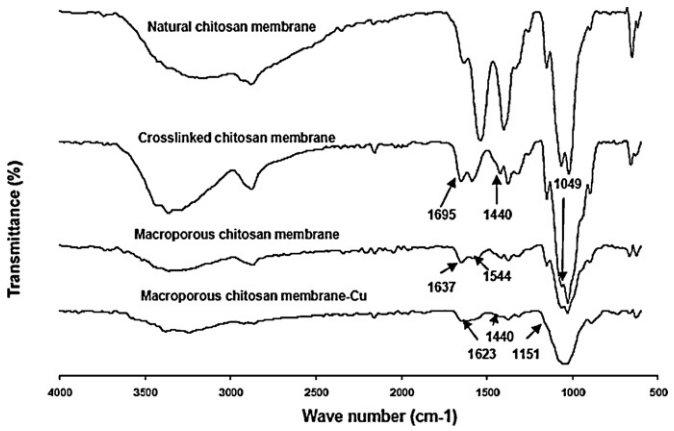

Fig. 1. ATR-FTIR spectra of different chitosan membranes.

3. Results and discussion

3.1. ATR-FTIR

During crosslinking using glutaraldehyde, amine groups of chitosan are converted into azomethine (C=N). Fig. 1 shows a reduction in the amine absorption at 1049 cm^{-1} and an increase in the imine absorption at 1440 cm^{-1} following the crosslinking step. This observation confirms that crosslinking occurred in the membrane. An increase in absorption at 1695 cm^{-1} is due to free aldehyde.

After preparation of the macroporous membrane, it is possible that a small amount of silica gel would remain in the membrane. However, a peak corresponding to silica was not observed in the spectra.

Table 1
Thickness and porosity of prepared membranes.

M*i*–*j*	Thickness (μm)	Porosity (%)
M3–0	89.473	
M3–1	121.052	8.05
M3–3	210.526	32.74
M4.5–0	123.684	
M4.5–1	178.947	11.23
M4.5–3	400	40.12
M6–0	163.150	
M6–1	289.473	17.68
M6–3	440	43.52

Comparing the spectra of the macroporous membrane before (macroporous chitosan membrane) and after Cu^{2+} adsorption (macroporous chitosan membrane–Cu), absorption peaks at 1151 cm^{-1} and 1440 cm^{-1} that correspond to stretching C–N and bending N–H are either weakened or totally vanished after Cu^{2+} adsorption. Therefore, these functional groups are considered to be involved in the metal adsorption, which further indicates that nitrogen atoms are the main adsorption sites for metal ions attachment [30,31]. Instead, a new absorption band appeared at 1600–1625 cm^{-1} considered as characteristic peak of chitosan–metal complex [31].

3.2. Thickness and porosity of membranes

Table 1 shows the thickness and porosity of the prepared membranes, M*i*–*j* (where *i* is the polymer concentration and *j* is the silica to chitosan ratio). Porosity is not reported for the membranes M*i*–0 since they are dense membranes and by definition porosity is supposed to be zero (see Eq. (6)). In membranes with the same polymer concentration, thickness and porosity increase when the silica to chitosan ratio is increased. With a constant silica to chitosan ratio,

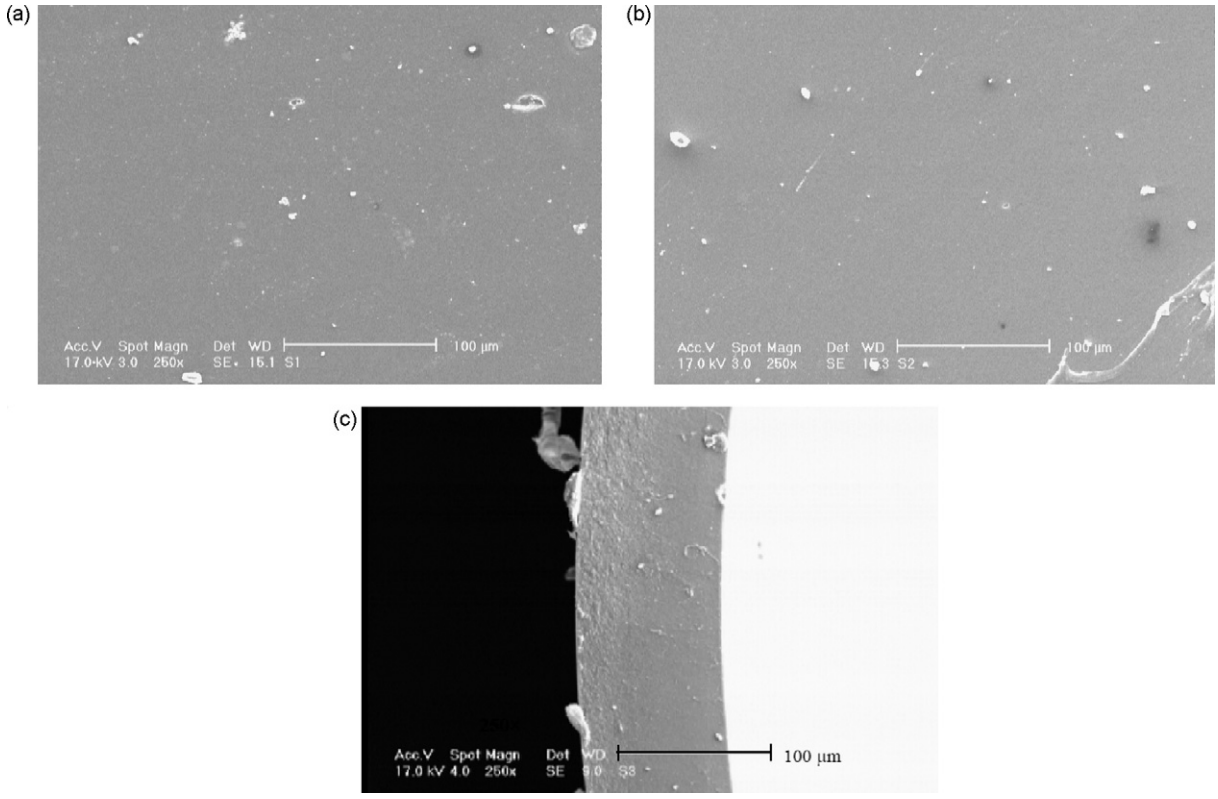

Fig. 2. (a) Top surface, (b) bottom surface and (c) cross-section of M3–0 with 250× magnification.

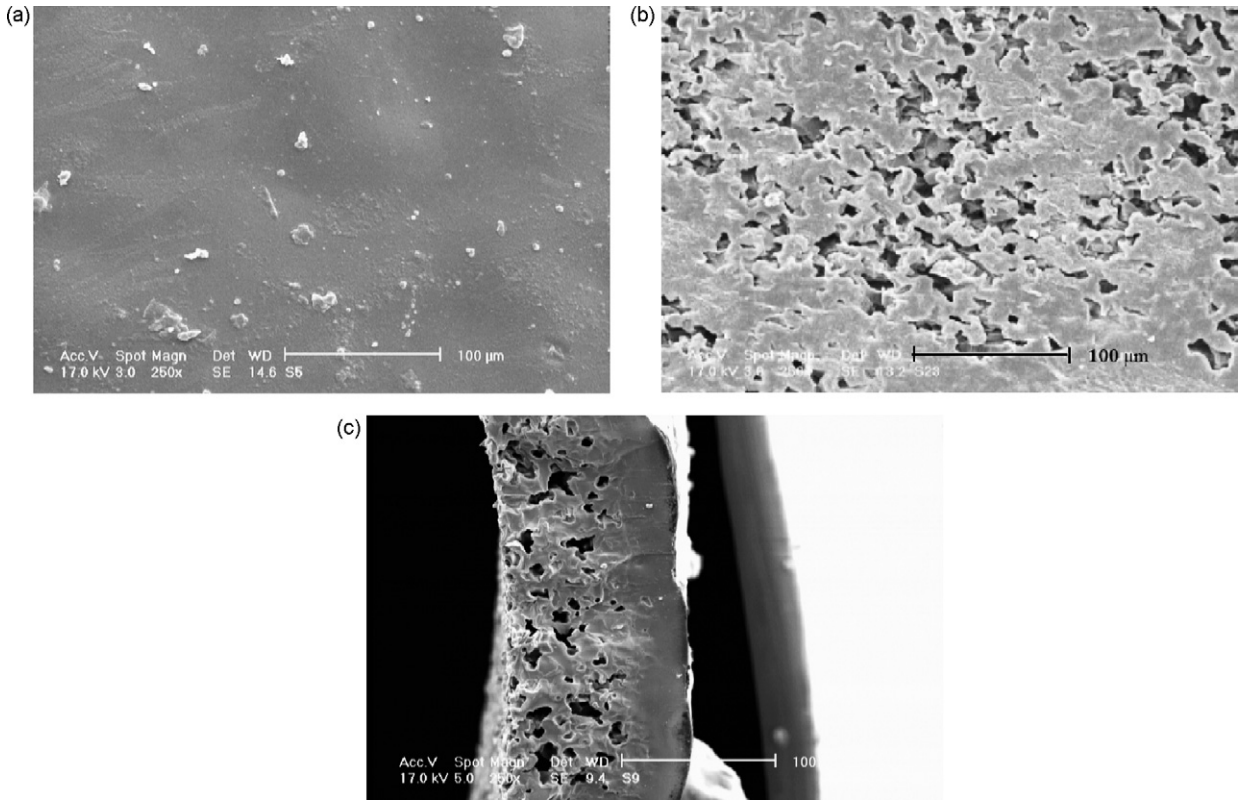

Fig. 3. (a) Top surface, (b) bottom surface and (c) cross-section of M3–1 with 250× magnification.

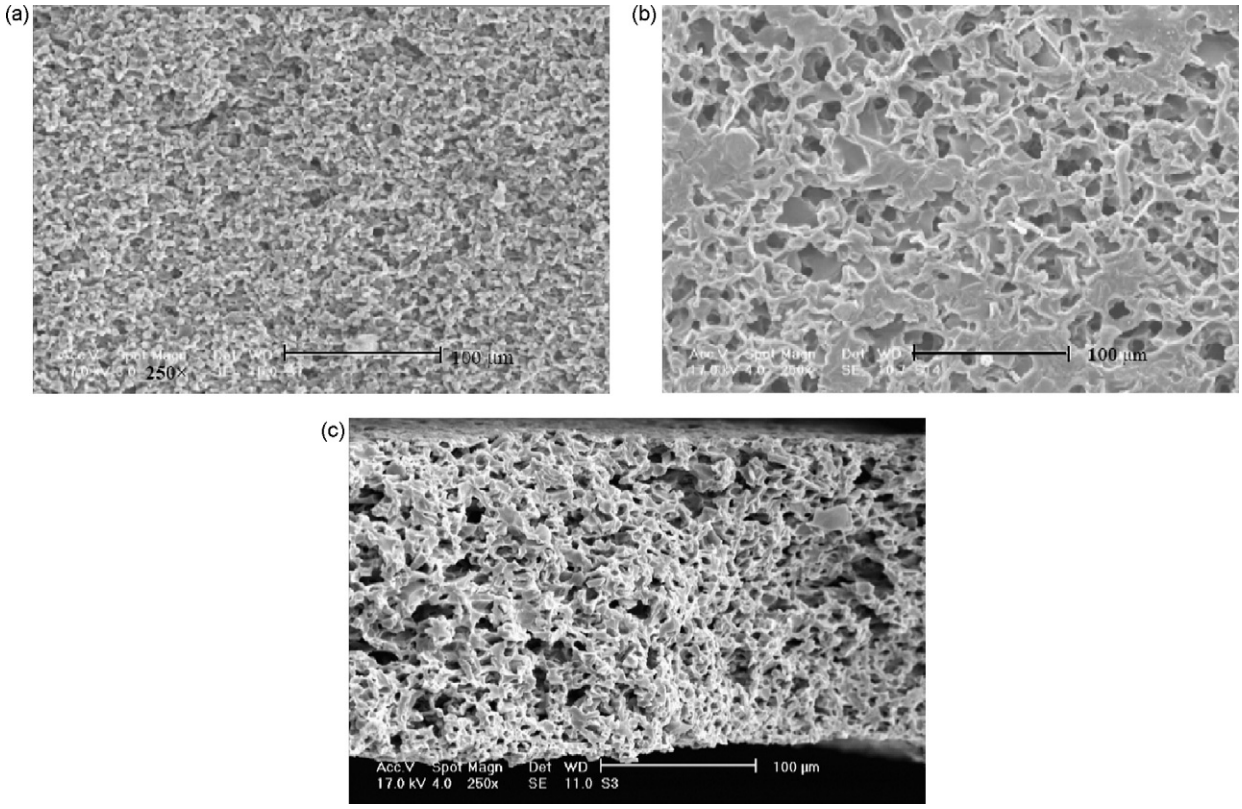

Fig. 4. (a) Top surface, (b) bottom surface and (c) cross-section of M3–3 with 250× magnification.

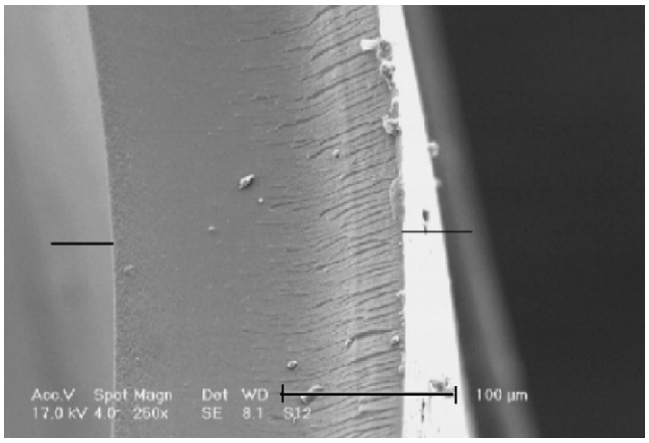

Fig. 5. Cross-section of M6–0 with 250× magnification.

thickness and porosity increase with increasing polymer concentration.

3.3. SEM–EDX analysis

The SEM images of the top and bottom surfaces and the cross-section of the membranes are given in Figs. 2–7.

3.3.1. The effect of polymer concentration

Comparing Figs. 2c and 5 show that the thickness of the dense membrane increased with an increase in polymer concentration. The same trend was observed for macroporous membranes.

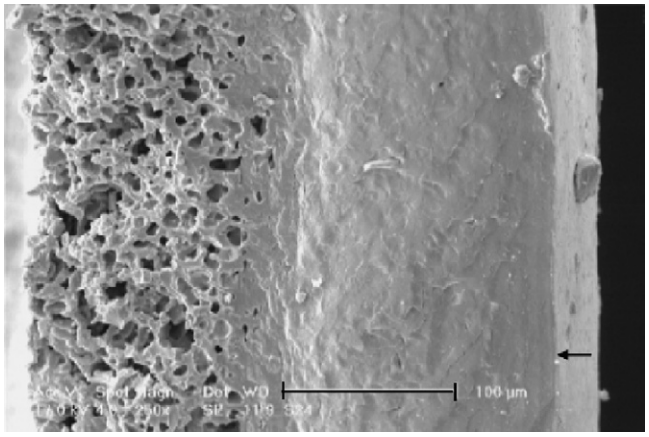

Fig. 6. Cross-section of M6–1 with 250× magnification.

Table 2
Surface roughness parameters of membranes.

Mi–*j*	S_z (nm)	S_a (nm)	S_q (nm)	S_{dq}	S_{dr} (%)
M6–0 top	20.3	1.99	2.58	0.035	0.062
M6–0 bottom	49.3	7.14	8.92	0.054	0.150
M6–1 top	67	7.32	9.21	0.088	0.380
M6–1 bottom	89.3	12.50	16.20	0.180	1.530
M6–3 top	609	139	187	0.710	21.900
M6–3 bottom	1880	145	286	1.310	66.500

3.3.2. The effect of silica to chitosan ratio

Figs. 2–4 show the SEM images of M3–*j* membranes where *j* increased progressively from 0 to 3. In the M3–0 membrane, both the top (Fig. 2a) and bottom (Fig. 2b) surfaces are dense. The cross-sectional image (Fig. 2c) also shows a dense structure. In the M3–1 membrane, the top surface (Fig. 3a) is dense while the bottom surface (Fig. 3b) is porous. The cross-sectional image (Fig. 3c) also shows the transition from the dense top to the porous bottom. Thus, this membrane has an asymmetric structure similar to the observation by Santos et al. [20]. Finally, the M3–3 membrane has a porous structure throughout, from the top to the bottom of the membrane (Fig. 4a–c). For membranes M6–*j*, the increase in j produced the same progressive change from dense to asymmetric to macroporous structure (Figs. 5–7).

3.3.3. Cu^{2+} adsorption to the membrane surface

Fig. 8a and b shows the SEM images of the top and the bottom surface of M6–3 membrane before Cu^{2+} adsorption, and Fig. 8c and d shows the same surfaces after Cu^{2+} adsorption. Star-shaped structures were formed after Cu^{2+} adsorption, with fewer but larger stars at the top surface. The presence of copper in the star-shaped structure was confirmed by the EDX spectra shown in Fig. 9. From the intensity of the copper peak, the weight percent of copper was determined to be 26.94% at the top surface and 45.14% at the bottom surface. The smaller number of star-shaped structures and the lower copper content at the top surface indicate that fewer adsorption sites are available at the top surface. The peak corresponding to Au is from the gold coating used for SEM characterization.

3.4. AFM analysis

Figs. 10 and 11 illustrate three-dimensional topography images of M6–0 top and bottom surface and M6–1 top surface. The digital data are summarized in Table 2 as roughness parameters. The magnitude of the roughness parameter depends on its definition, but some common features are observed in all the reported parameters.

(1) For all M6–*j* membranes, the roughness parameter of the bottom surface is greater than that of the top surface. This is

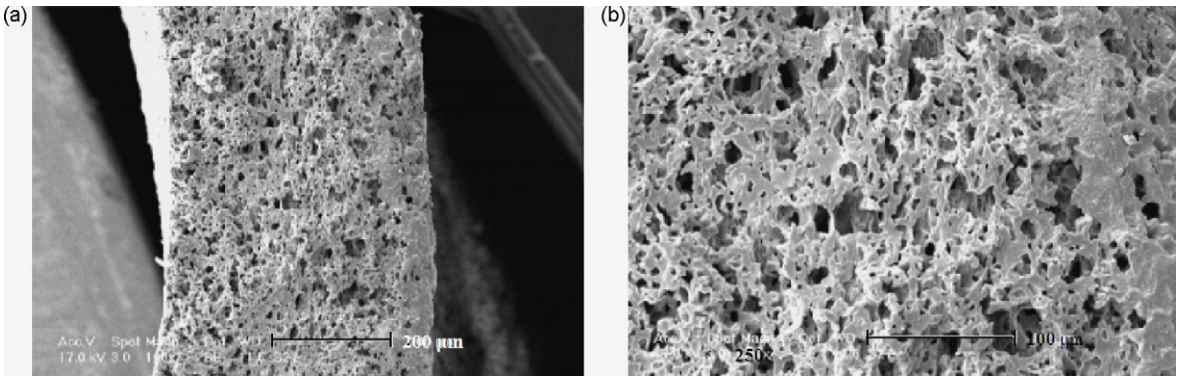

Fig. 7. Cross-section of M6–3 with 100× and 250× magnifications.

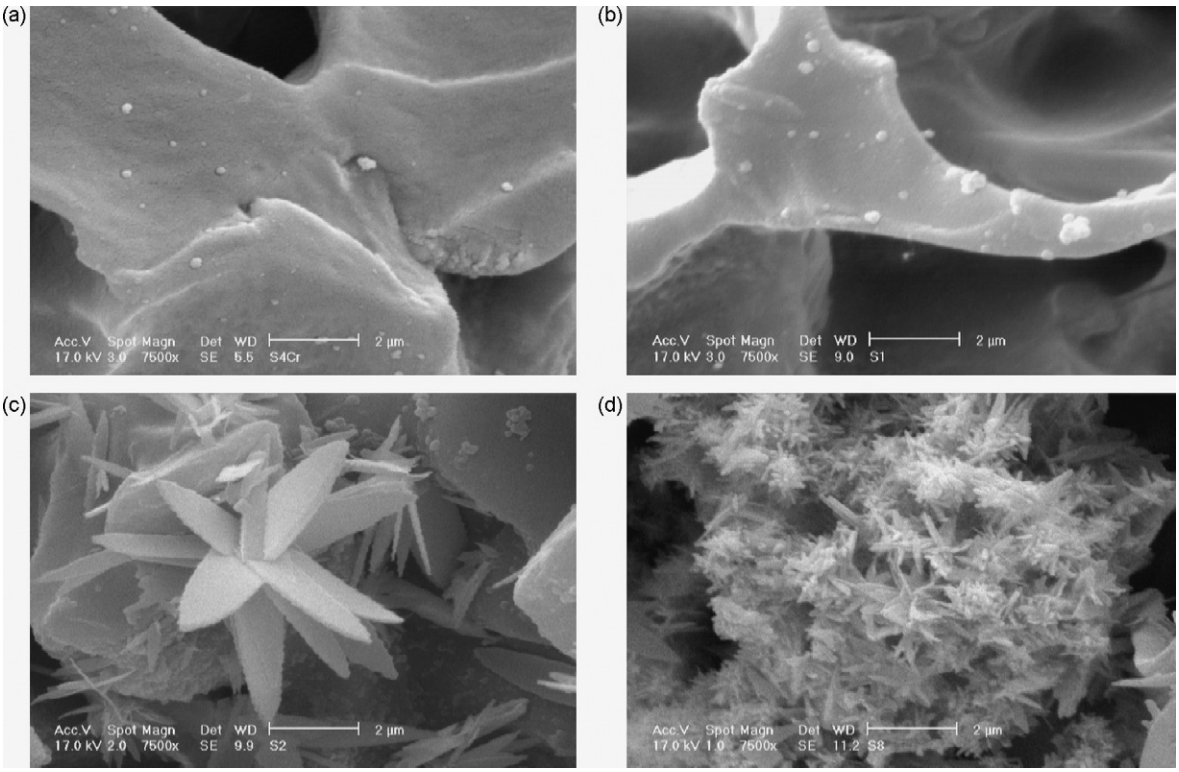

Fig. 8. (a) Top surface and (b) bottom surface of M6–3 before adsorption. (c) Top surface and (d) bottom surface of M6–3 after adsorption with 7500× magnification.

understandable for the M6–1 membrane that has an asymmetric structure. But it is interesting that the same trend is observed for the dense M6–0 membrane that is supposed to be "homogeneous" across the cross-section, and for the M6–3 membrane that is macroporous across the cross-section.

(2) The surface roughness increases as the silica content increases from 0 to 3. This is in accordance with the increase in porosity caused by the increased silica content.

The last column of Table 2 shows S_{dr} that indicates the percent increase in the effective surface area of adsorption as compared to the nominal surface area. Notably, the M6–3 membrane, which has the highest roughness parameter, shows a gain of approximately 90% in the effective surface area when the top and bottom surfaces are combined.

Table 3
Copper adsorption amount of membranes after 24 h.

M*i–j*	Copper ion adsorption amount (mg/g)
M3–0	2.696
M3–1	2.716
M3–3	4.400
M4.5–0	2.735
M4.5–1	2.936
M4.5–3	5.257
M6–0	3.040
M6–1	3.402
M6–3	5.900

3.5. Copper adsorption on chitosan membranes

Table 3 lists the amounts of copper adsorbed on different membranes at C_0 = 125 ppm. Higher adsorption amounts are associated

Table 4
The Freundlich and Langmuir constants for copper–chitosan adsorption.

	Freundlich model			
M*i–j*	K_F ($mg^{1-1/n}\,g^{-1}\,L^{1/n}$)	n	R^2	STD[a]
M6–0	0.864	4.629	0.988	2.64
M6–1	0.832	4.311	0.984	2.81
M6–3	0.831	4.444	0.941	3.20

	Langmuir model				
M*i–j*	K_L (L/g)	a_L (mg/L)	q_m (mg/g)	R^2	STD[a]
M6–0	0.053	0.0030	17.660	0.762	4.33
M6–1	0.107	0.0041	26.097	0.947	3.65
M6–3	0.390	0.0083	46.980	0.972	3.49

[a] Standard deviation $\left(\mathrm{STD} = 100 \times \sqrt{\frac{1}{N}\sum_{i=1}^{N}\frac{(q_{exp}-q_{cal})^2}{q_{exp}}}\right)$ [32].

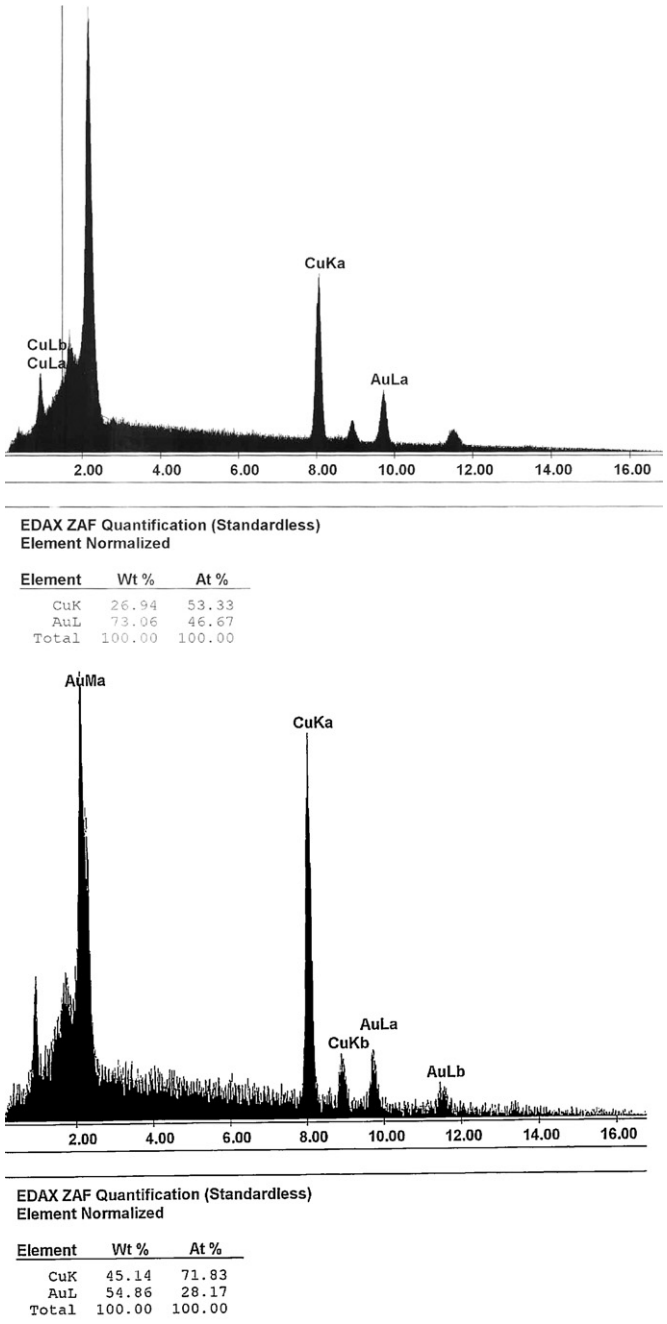

Fig. 9. EDX spectra of M6–3 after adsorption: (a) upper layer and (b) lower layer.

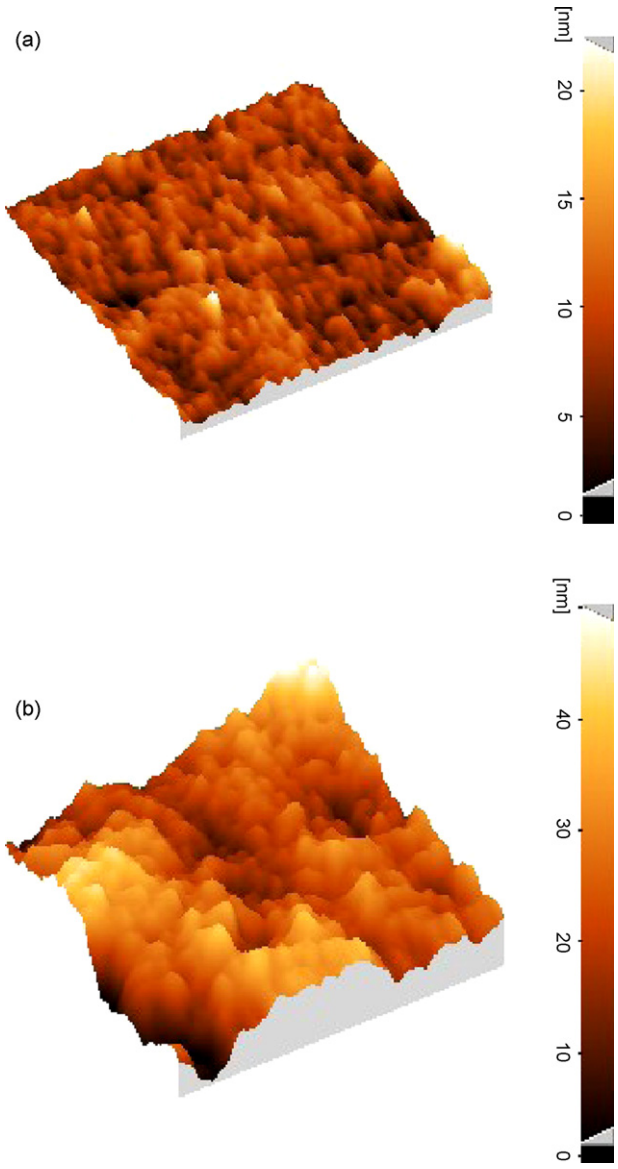

Fig. 10. 3D topography image of (a) top and (b) bottom surface of M6–0.

with higher polymer concentrations in the casting solution. The adsorbed amounts of copper also increase when the silica to chitosan ratio is raised from 0/1 to 3/1. This higher ratio results in greater porosity (Table 1) and roughness (e.g. Table 2 for M6–*j* membranes), making more amino groups available for chelation with copper ions.

Fig. 12 plots copper adsorption amount versus equilibrium concentrations for M6–0, M6–1 and M6–3 membranes. The amount of copper adsorbed increases as the concentration of copper in the solution increases, and greater adsorption is observed for membranes with higher silica to chitosan ratios. The correlation of equilibrium data by Freundlich and Langmuir equations was investigated and the associated parameters and their standard deviations are reported in Table 4. The equations are as follows [33]:

Freundlich model:

$$q = K_F\ C_{eq}^{1/n} \tag{12}$$

where K_F ($mg^{1-1/n}\ g^{-1}\ L^{1/n}$) and n are the Freundlich isotherm constants; q and C_{eq} are adsorption amount and metal concentration at equilibrium. This equation is derived by assuming a heterogeneous surface with the nonuniform distribution of the heat of adsorption over the surface.

Langmuir model:

$$\frac{C_{eq}}{q} = \frac{1}{K_L\ q_m} + \frac{C_{eq}}{q_m} \tag{13}$$

where q_m (mg/g) and K_L (L/mg) are the maximum adsorption capacity and the Langmuir isotherm constant; q and C_{eq} are adsorption amount and metal concentration at equilibrium. This equation assumes that the surface of the pores of adsorbent is homogenous and the forces of interaction between adsorbed molecules are negligible.

The Freundlich model shows a better fit to the adsorption data. Also it can be observed that M6–3 has a maximum adsorption capacity of 46.98 mg/g. Transition metals are mainly adsorbed via

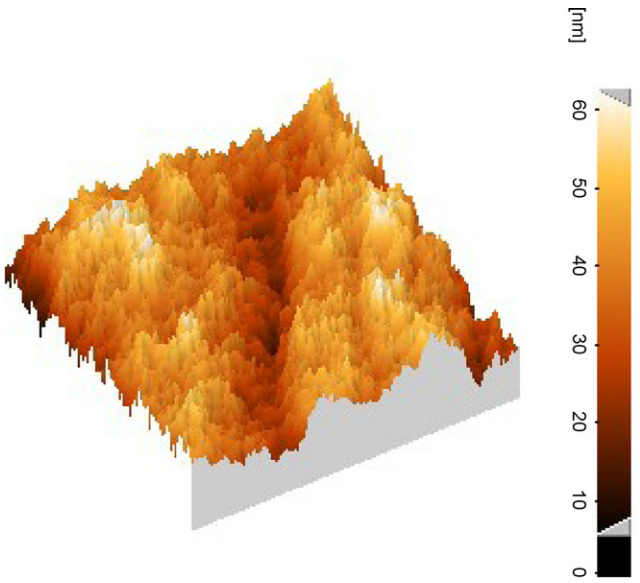

Fig. 11. 3D topography image of top surface of M6–1.

coordination with the NH_2 groups on chitosan. Verbych et al. reported that about 20% of the amino group of chitosan is protonated even at pH 6.9 and the reactions in Eqs. (1) and (2) compete during adsorption [34].

Muzzareli et al. investigated the chelation of Cu^{2+} with chitosan membranes by ultraviolet, infra-red and electron spin resonance. They realized that the average number of amino groups bound to one heavy metal ion changes with solution pH. At pH 5 because of the larger extent of protonated amino groups, about one to two amino groups bind with Cu^{2+}. The number of amino groups bound may increase up to two to three at pH 5–6. At pH 6–8, three amino groups and one hydroxyl group would bind with one Cu^{2+} [34].

Experiments revealed that the pH becomes always larger after adsorption [35]. The zeta potential (ζ) of the biopolymer varies from positive to negative as the pH increases. The dependence of background electrolyte concentration and counter ions present in solution on zeta potential is well known. It can be assumed that a high concentration of SO_4^{2-} in the electrolyte causes adsorption of these anions by polymer and decreases the positive value of the ζ. Consequently, chitosan possesses a negatively charged characteristic and shows additional ability to increase its uptake capacity to Cu^{2+} (electrostatic mechanism) [34].

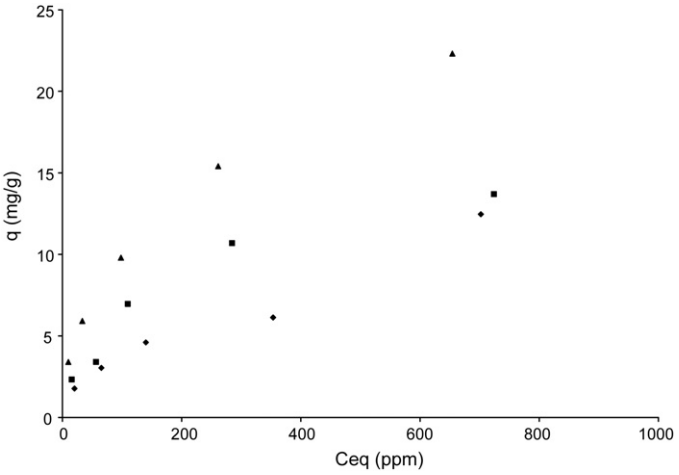

Fig. 12. Equilibrium copper ion adsorption amount (q_e) for (♦) M6–0, (■) M6–1, (▲) M6–3 versus the equilibrium copper ion concentration (C_{eq}) in the solution.

Table 5
The pseudo-first and second order kinetic parameters for copper–chitosan adsorption.

	Pseudo-first order model			
Mi–j	k_1	q_e (mg/g)	R^2	STD
M6–0	0.0023	1.84	0.975	3.54
M6–1	0.0023	1.82	0.906	4.51
M6–3	0.0018	1.75	0.975	3.06
	Pseudo-second order model			
Mi–j	k_2 (g mg^{-1} min^{-1})	q_e (mg/g)	R^2	STD
M6–0	0.00047	6.32	0.991	2.19
M6–1	0.00084	7.72	0.992	1.43
M6–3	0.00120	10.2	0.997	1.27

The fact that Freundlich model fits better than Langmuir model indicates that monolayer biosorption as well as heterogeneous surface conditions may coexist under the applied experimental conditions. Therefore, the adsorption behaviour of copper ions is complex and it involves more than one mechanism including chelation and electrostatic adsorption. This has been observed by different researches [12,17,35–38].

Kinetic data indicate that 24 h (1440 min) of adsorption time is sufficient to reach the adsorption equilibrium. To investigate the mechanism of sorption kinetics, models have been used to test experimental data. The pseudo-first and second order kinetic models [9] have been developed to fit experimental adsorption kinetic results.

The pseudo-first order equation of Lagergren is expressed as follows:

$$\log(q_e - q_t) = \log(q_e) - \frac{k_1}{2.303}t \tag{14}$$

where q_e and q_t are the sorption amount (mg/g) at equilibrium and at time t (min), respectively and k_1 is the rate constant of pseudo-first order sorption (1/min).

The pseudo-second order equation is expressed as follows:

$$\frac{t}{q_t} = \frac{1}{k_2 q_e^2} + \frac{1}{q_e}t \tag{15}$$

where q_e and q_t are the sorption amount (mg/g) at equilibrium and at time t (min), respectively and k_2 is the rate constant of pseudo-second order sorption (g mg^{-1} min^{-1}).

The constants are presented in Table 5. It is obvious that the adsorption of copper ions onto membranes fits well with the pseudo-second order kinetic model and chemisorption is the rate limiting step. As previously explained the copper adsorption mechanism is the combination of chelation and electrostatic adsorption. From the kinetic data it can be found out that the chelation is dominant. The pseudo-first and second order kinetic models have been the most widely tested models for the sorption of copper ions from wastewater [9,21,39–42]. Most of the fit for pseudo-first order model are moderate to poor. In these literatures the pseudo-second order model for chitosan–copper ion systems provide an exceptionally high degree of correlation between the model results and the experimental data (Table 6).

3.6. Membrane reuse

Table 4 showed the experimental results on the amount of copper ions adsorbed and the percentage of desorption in three cycles. It was observed that the adsorption capacities of copper ions decreased slightly after each cycle. The results indicated

Table 6
Chitosan membranes regeneration during adsorption/desorption cycles.

	Cycle 1		Cycle 2		Cycle 3	
	Uptake (mg/g)	Desorption percent (%)	Uptake (mg/g)	Desorption percent (%)	Uptake (mg/g)	Desorption percent (%)
M6–0	4.60	77.35	3.74	72.91	3.04	73.84
M6–1	6.96	81.02	5.93	79.45	5.36	76.89
M6–3	9.82	85.18	8.57	82.63	7.61	79.56

that the chitosan membranes can be recovered for consecutive uses.

4. Conclusions

Dense and porous chitosan membranes were prepared for copper ion adsorption. Since adsorption experiments were carried out in batch processes, the external surfaces and their functional groups were extensively exposed to copper ions and so these surfaces played a more important role than the inner parts. By increasing polymer concentration, more amine groups were available for chelation and as a result copper adsorption increased. Increasing the silica to chitosan ratio of the membrane leads to higher porosity and roughness, as measured by AFM. High porosity and consequently higher roughness of prepared membranes resulted in a greater surface area, which also lead to increased copper adsorption. A silica to chitosan ratio of 1/1 produced asymmetric membranes; further increase of the ratio to 3/1 leads to approximately symmetric membrane as observed by SEM. While both amine group availability and its amount contributed to better ion adsorption, the availability of amine functional groups had a more pronounced effect.

References

[1] Y.S. Ho, G. Mckay, Sorption of copper (II) from aqueous solution by peat, Water Air Soil Pollut. 158 (2004) 77–97.
[2] B. Kannamba, K.L. Reddy, B.V. Apparao, Removal of Cu(II) from aqueous solutions using chemically modified chitosan, J. Hazard. Mater. 175 (2010) 939–948.
[3] F.C. Wu, R.L. Tseng, R.S. Juang, A review and experimental verification of using chitosan and its derivatives as adsorbents for selected heavy metals, J. Environ. Manage. 91 (2009) 798–806.
[4] K.R. Krishnapriya, M. Kandaswamy, Synthesis and characterization of a crosslinked chitosan derivative with complexing agent and its adsorption studies towards metal(II) ions, Carbohyd. Res. 334 (2009) 1632–1638.
[5] A.T. Paulino, F.A.S. Minasse, M.R. Guilherme, A.V. Reis, E.C. Muniz, J. Nozaki, Novel adsorbent based on silkworm chrysalides for removal of heavy metals from wastewaters, J. Colloid Interface Sci. 301 (2006) 479–487.
[6] S. Babel, T.A. Kurniawan, Low-cost adsorbents for heavy metals uptake from contaminated water: a review, J. Hazard. Mater. B97 (2003) 219–243.
[7] E. Guibal, Interactions of metal ions with chitosan-based sorbents: a review, Sep. Purif. Technol. 38 (2004) 43–74.
[8] L. Jin, R. Bai, Mechanisms of lead adsorption on chitosan/PVA hydrogel beads, Langmuir 18 (2002) 9765–9770.
[9] A.R. Cestari, E.F.S. Vieira, J.D.S. Matos, F.S.C. Anjos, Determination of kinetic parameters of Cu(II) interaction with chemically modified thin chitosan membranes, J. Colloid Interface Sci. 285 (2005) 288–295.
[10] R.S. Vieira, E. Guibal, E.A. Silva, M.M. Beppu, Adsorption and desorption of binary mixtures of copper and mercury ions on natural and crosslinked chitosan membranes, Adsorption 13 (2007) 603–611.
[11] E.C.N. Lopes, F.S.C. Anjos, E.F.S. Vieira, A.R. Cestari, An alternative Avrami equation to evaluate kinetic parameters of the interaction of Hg(II) with thin chitosan membranes, J. Colloid Interface Sci. 263 (2003) 542–547.
[12] P. Baroni, R.S. Vieira, E. Meneghetti, M.G.C. Silva, M.M. Beppu, Evaluation of batch adsorption of chromium ions on natural and crosslinked chitosan membranes, J. Hazard. Mater. 152 (2008) 1155–1163.
[13] R.S. Vieira, M.M. Beppu, Dynamic and static adsorption and desorption of Hg(II) ions on chitosan membranes and spheres, Water Res. 40 (2006) 1726–1734.
[14] R.S. Vieira, M.M. Beppu, Interaction of natural and crosslinked chitosan membranes with Hg(II) ions, Colloids Surf. A 279 (2006) 196–207.
[15] R.S. Vieira, M.M. Beppu, Mercury ion recovery using natural and crosslinked chitosan membranes, Adsorption 11 (2005) 731–736.
[16] M.M. Beppu, E.J. Arruda, R.S. Vieira, N.N. Santos, Adsorption of Cu(II) on porous chitosan membranes functionalized with histidine, J. Membr. Sci. 240 (2004) 227–235.
[17] X.P. Wang, Z.Q. Shen, Studies on the effects of copper salts on the separation performance of chitosan membranes, Polym. Int. 49 (2000) 1426–1433.
[18] W. Kamiński, Z. Modrzejewska, Separation of Cr(VI) on chitosan membranes, Ind. Eng. Chem. Res. 38 (1999) 4946–4950.
[19] W. Kamiński, Z. Modrzejewska, Application of chitosan membranes in separation of heavy metal ions, Sep. Sci. Technol. 32 (1997) 2659–2668.
[20] D.E.S. Santos, C.G.T. Neto, J.L.C. Fonseca, M.R. Pereira, Chitosan macroporous asymmetric membranes: preparation, characterization and transport of drugs, J. Membr. Sci. 325 (2008) 362–370.
[21] A.C. Chao, S.H. Yu, G.S. Chuang, Using NaCl particles as porogen to prepare a highly adsorbent chitosan membranes, J. Membr. Sci. 280 (2006) 163–174.
[22] R.L. Machado, E.J. Arruda, C.C. Santana, S.M.A. Bueno, Evaluation of a chitosan membrane for removal of endotoxin from human IgG solutions, Process Biochem. 41 (2006) 2252–2257.
[23] M. Gumusderelioglu, P. Agi, Adsorption of concanavalin A on the well-characterized macroporous chitosan and chitin membranes, React. Funct. Polym. 61 (2004) 211–220.
[24] X. Zeng, E. Ruckenstein, Control of pore sizes in macroporous chitosan and chitin membranes, Ind. Eng. Chem. Res. 35 (1996) 4169–4175.
[25] J. Barzin, S.S. Madaeni, H. Mirzadeh, M. Mehrabzadeh, Effect of polyvinylpyrrolidone on morphology and performance of hemodialysis membranes prepared from polyether sulfone, J. Appl. Polym. Sci. 92 (2004) 3804–3813.
[26] T.Y. Hsien, G.L. Rorrer, Effects of acylation and crosslinking on the material properties and cadmium ion adsorption capacity of porous chitosan beads, Sep. Sci. Technol. 30 (1995) 2455–2475.
[27] Z.Y. Gu, P.H. Xue, W.J. Li, Preparation of porous chitosan membrane by cryogenic induced phase separation, Polym. Adv. Technol. 12 (2001) 665–669.
[28] K.C. Khulbe, C. Feng, T. Matsuura, Synthetic Polymeric Membranes: Characterization by Atomic Force Microscopy, Springer, 2008.
[29] J. Barzin, C. Feng, K.C. Khulbe, T. Matsuura, S.S. Madaeni, H. Mirzadeh, Characterization of polyethersulfone hemodialysis membrane by ultrafiltration and atomic force microscopy, J. Membr. Sci. 237 (2004) 77–85.
[30] W.S. Wan Ngah, S. Fatinathan, Adsorption characterization of Pb(II) and Cu(II) ions onto chitosan-tripolyphosphate beads: kinetic, equilibrium and thermodynamic studies, J. Environ. Manage. 91 (2010) 958–969.
[31] X. Wang, Y. Du, F. Lihong, H. Liu, Y. Hu, Chitosan–metal complexes as antimicrobial agent: synthesis, characterization and structure–activity study, Polym. Bull. 55 (2005) 105–113.
[32] F.C. Wu, R.L. Tseng, R.S. Juang, Kinetic modelling of liquid-phase adsorption of reactive dyes and metal ions on chitosan, Water Res. 35 (2001) 613–618.
[33] A. Shafaei, F. Zokaee Ashtiani, T. Kaghazchi, Equilibrium studies of the sorption of Hg(II) ions onto chitosan, Chem. Eng. J. 133 (2007) 311–316.
[34] S. Verbych, M. Bryk, G. Chornokur, Removal of copper (II) from aqueous solutions by chitosan adsorption, Sep. Sci. Technol. 40 (2005) 1749–1759.
[35] R.S. Juang, H.J. Shao, Effect of pH on competitive adsorption of Cu(II), Ni(II), and Zn(II) from water onto chitosan beads, Adsorption 8 (2002) 71–78.
[36] W.S. Wan Ngah, S. Fatinathan, Pb(II) biosorption using chitosan and chitosan derivatives beads: equilibrium, ion exchange and mechanism studies, J. Environ. Sci. 22 (2010) 338–346.
[37] J. Cao, Y. Tan, Y. Che, H. Xin, Novel complex gel beads composed of hydrolyzed polyacrylamide and chitosan: an effective adsorbent for the removal of heavy metal from aqueous solution, Bioresour. Technol. 101 (2010) 2558–2561.
[38] T. Gotoh, K. Matsushima, K.I. Kikuchi, Preparation of alginate–chitosan hybrid gel beads and adsorption of divalent metal ions, Chemosphere 55 (2004) 135–140.
[39] W.S. Wan Ngah, A. Kamari, Y.J. Koay, Equilibrium and kinetics studies of adsorption of copper (II) on chitosan and chitosan/PVA beads, Int. J. Biol. Macromol. 34 (2004) 155–161.
[40] C. Liu, R. Bai, Adsorptive removal of copper ions with highly porous chitosan/cellulose acetate blend hollow fiber membranes, J. Membr. Sci. 284 (2006) 313–322.
[41] Y. Sag, Y. Aktay, Kinetic studies on sorption of Cr(VI) and Cu(II) ions by chitin, chitosan and Rhizopus arrhizus, Biochem. Eng. J. 12 (2002) 143–153.
[42] W.H. Cheung, J.C.Y. Ng, G. McKay, Kinetic analysis of the sorption of copper(II) ions on chitosan, J. Chem. Technol. Biotechnol. 78 (2003) 562–571.